Catalysis Science & Technology

ROYAL SOCIETY OF CHEMISTRY

PAPER

Cite this: *Catal. Sci. Technol.*, 2022, 12, 5171

Nano-sized H-ZSM-5 zeolite catalyzes aldol condensation reaction to prepare methyl acrylate and acrylic acid†

Mingguan Xie,[abc] Youming Ni, *[ab] Xudong Fang,[abc] Hongchao Liu,[ab] Zhiyang Chen,[ab] Xiangnong Ding,[abc] Linying Wang[ab] and Wenliang Zhu *[ab]

The aldol condensation reaction of formaldehyde and methyl acetate is generally considered as a green, economical, non-petroleum route for one-step production of methyl acrylate (MA) and acrylic acid (AA). However, conventional aldol condensation catalysts are prone to rapid deactivation due to severe coking and quick loss of catalytic centers caused by acidic products and water. Here, we report an efficient and long-term stable nano-sized N-H-ZSM-5 zeolite catalyst for this condensation reaction. Its total lifetime reaches up to 226 h by three regeneration runs with the MA and AA formation rate being more than 0.9 mmol g^{-1} h^{-1} with the programmed temperature rising from 563 K to 663 K. After each regeneration, the aldol condensation activity and the single-pass lifetime of the N-H-ZSM-5 zeolite catalyst increased unexpectedly under the same reaction conditions. The results from a variety of characterization methods prove that the large capacity to hold big-sized polyaromatic coke, the good structural stability during the reaction and regeneration and the gradually improved diffusion performance after regeneration lead to the excellent performances of the nano-sized N-H-ZSM-5 catalyst during the aldol condensation reaction of formaldehyde and methyl acetate. This exhibits potential for development of a new route for MA and AA synthesis with non-petroleum resources.

Received 7th March 2022,
Accepted 26th June 2022

DOI: 10.1039/d2cy00447j

rsc.li/catalysis

1. Introduction

Methyl acrylate (MA) and acrylic acid (AA), widely used as polymer monomers for preparation of coatings, paints, carbon fibers, adhesives, *etc.*, are important oxygenated chemicals[1] and mainly produced through two-step oxidation of propylene which heavily relies on increasingly depleted oil resources.[2] However, there is a risk of explosion in the oxidation of propylene with air/oxygen, which limits the wide application of this route. In addition, due to the over-oxidation of propylene during the reaction, low selectivity to AA and MA is inevitable, resulting in the poor atom economy of the oxidation route.[3] Therefore, it is of great significance to develop a green, economical, non-petroleum route for production of MA and AA.

In recent years, the one-step aldol condensation reaction of formaldehyde (HCHO) and methyl acetate (MAc) is generally considered as a promising alternative route to produce MA and AA.[4] The feedstocks HCHO and MAc have been industrially synthesized with non-petroleum platform chemical methanol, which can be derived from coal, natural gas, biomass, or even carbon dioxide.[5] Moreover, according to the condensation reaction mechanism, the formation of carbon–carbon bonds generally occurs at a specific location, which will result in a higher target product selectivity.[6,7] Many previous studies have reported that the aldol condensation reaction can be catalyzed by solid base or base–acid bifunctional catalysts.[8–17] Solid base catalysts such as alkali metals or alkaline earth metals supported on SiO_2 or Al_2O_3 carriers can achieve high selectivity for MA and AA. However, these catalysts deactivate rapidly and their single-pass lifetimes are short, meanwhile the loss of basic catalytic centers caused by acidic products and water will make the entire lifetimes of these catalysts short.[8–12] Base–acid bifunctional catalysts such as V_2O_5–P_2O_5 systems also suffer from the same problem above.[13–17]

Zeolite is a kind of crystalline material with stable and porous structure, which can be resistant to acid and water generated in the aldol condensation reaction.[18] Therefore, zeolites are often used as carriers to support active sites such as Cs and P species during aldol condensation catalyst preparation.[19,20] However, the loss of these active sites could also be unavoidable due to the same reasons mentioned

[a] *National Engineering Research Center of Lower-Carbon Catalysis Technology, Dalian Institute of Chemical Physics, Chinese Academy of Sciences, Dalian 116023, Liaoning, China. E-mail: niyouming@dicp.ac.cn, wlzhu@dicp.ac.cn*
[b] *Dalian National Laboratory for Clean Energy, Dalian 116023, Liaoning, China*
[c] *University of Chinese Academy of Sciences, Beijing 100049, China*

† Electronic supplementary information (ESI) available. See DOI: https://doi.org/10.1039/d2cy00447j

above. H-Type zeolites are rich in Brønsted acid sites, which are also active for the condensation reaction.[21] Our previous work found that H-ZSM-35 zeolite demonstrated an excellent selectivity in the aldol condensation of methyl acetate with dimethoxymethane.[4] Nevertheless, the stability of the H-ZSM-35 zeolite catalyst is unsatisfactory and the single-pass lifetime is less than 9 hours. Another study from our group has proven that the H-type zeolites can readily catalyze the conversion of formaldehyde to polyaromatics and coke, which quickly leads to deactivation.[22] Therefore, improving the coke resistance and the stability of H-type zeolites is the key to industrialization for the condensation reaction to produce MA and AA.

Here, we report a nano-sized N-H-ZSM-5 zeolite catalyst, which presents an excellent stability in the condensation reaction of MAc and HCHO at 0.1 MPa and MAc/HCHO = 5/1 (molar ratio). The total lifetime reaches up to 226 h by three regeneration runs. More interestingly, the activity and stability are further improved after each regeneration cycle.

2. Experimental

2.1. Materials

Nano-sized and micro-sized H-ZSM-5 zeolites with various SiO_2/Al_2O_3 ratios (N-H-ZSM-5, N-H-ZSM-5-H, and M-H-ZSM-5), H-beta, H-ZSM-35, and H-MOR zeolites were provided commercially, which were the same as those in our previous studies.[23–25] The deactivated N-H-ZSM-5 in Fig. 2A was regenerated by calcination in air at 823 K for 3 h, and the sample regenerated 4 times finally was denoted as N-H-ZSM-5-Re.

2.2. Catalytic tests

The aldol condensation reaction experiments were performed in a fixed-bed stainless steel tubular reactor with 8 mm inner diameter. The catalyst (0.5 g, 40–60 mesh) was packed in the reactor and activated at 673 K under N_2 for 2 h. The reaction was performed under atmospheric pressure. The mixed solution of methyl acetate (MAc) and formaldehyde (trioxane was used as the source of the formaldehyde) was steadily

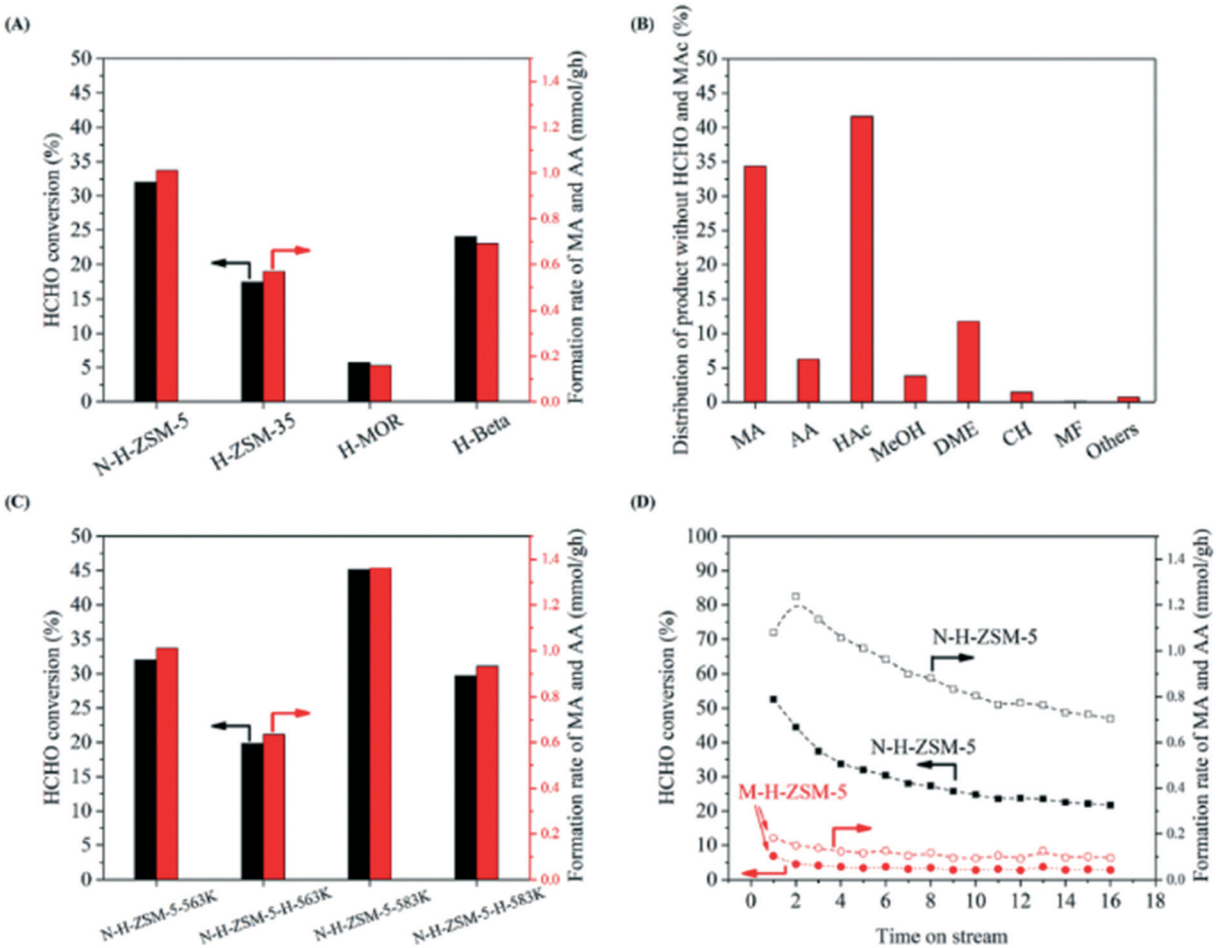

Fig. 1 The catalytic performances of zeolite catalysts in the aldol condensation reaction of HCHO and MAc. Reaction conditions: 0.5 g catalyst, 1 atm, TOS = 5 h, n_{MAc}/n_{HCHO} = 5/1, WHSV = 1.4 g g^{-1} h^{-1}. (A) Comparison of results over various zeolite catalysts at 563 K. (B) Distribution of products over the N-H-ZSM-5 catalyst at 563 K, including methyl acrylate (MA), acrylic acid (AA), acetic acid (HAc), methanol (MeOH), dimethyl ether (DME), hydrocarbons (CH), methyl formate (MF) and other compounds (others). (C) Comparison of results over N-H-ZSM-5 with different SiO_2/Al_2O_3 ratios at 563 K and 583 K. (D) Comparison of results over H-ZSM-5 with different crystal sizes.

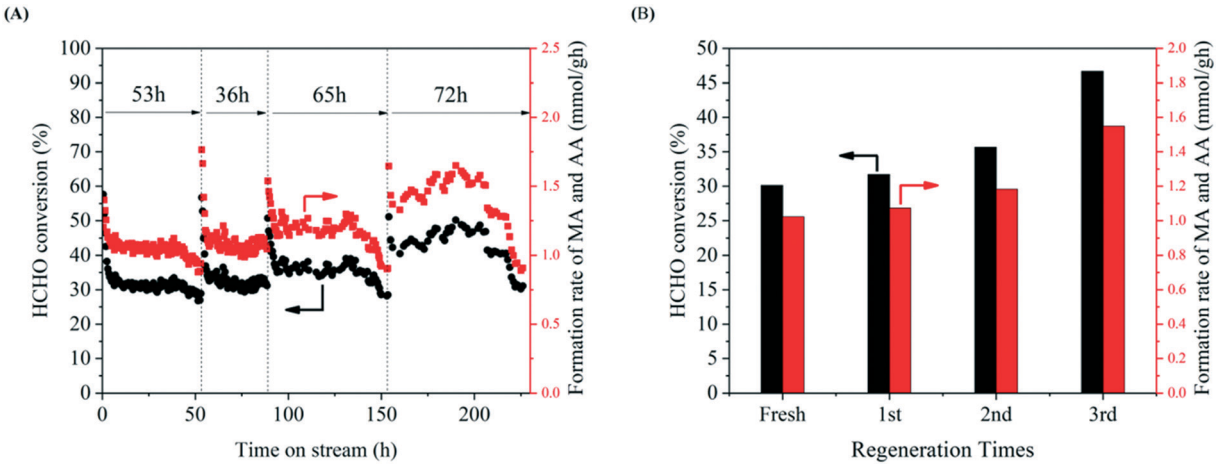

Fig. 2 Stability test for the aldol condensation reaction over fresh and regenerated N-H-ZSM-5. (A) The catalytic results for the N-H-ZSM-5 zeolite catalyst. (B) Comparison of catalytic results at approximately 25 h on stream after each regeneration. Reaction conditions: the programmed temperature (563 K for 90 min, ramp 1 K per 30 min to 578 K, ramp 1 K per 60 min to 598 K, ramp 1 K per 45 min to 645 K and finally ramp 1 K per 30 min to the end of the reaction, also see in Fig. S2†), 0.1 MPa, n_{MAc}/n_{HCHO} = 5/1, WHSV = 1.4 h^{-1}.

pumped into the reactor by a pump. The weight hourly space velocity (WHSV) of the mixed solution was 1.4 g $g_{cat.}^{-1}$ h^{-1}. The molar ratio of MAc and formaldehyde was fixed at 5. The flow of carrier gas N_2 is 50 mL min^{-1}. All the reaction products were analyzed using an online gas chromatograph (Agilent 7890A) equipped with an FFAP capillary column connected to a flame ionization detector (FID) and a Porapak T column connected to a thermal conductivity detector (TCD). MA was used as a reference bridge between the TCD and FID. The HCHO conversion and formation rate of MA and AA were calculated with the following equations.

$$\text{HCHO conversion} = \frac{3\times\text{trioxane moles at the inlet} - \text{HCHO moles at the outlet}}{3\times\text{trioxane moles at the inlet}}\times 100\% \quad (1)$$

$$\text{Formation rate of MA and AA } \left(\text{mmol } g_{cat.}^{-1}\ h^{-1}\right) = \frac{\text{C moles of feed rates } \left(\text{mmol C } h^{-1}\right)}{\text{grams of catalyst (g)}}\times\left(\frac{\text{C moles of MA}}{\text{C moles of products}\times 4}+\frac{\text{C moles of AA}}{\text{C moles of products}\times 3}\right)\times 100\% \quad (2)$$

2.3. Catalysts characterization

A PANalytical X' Pert Pro diffractometer with Cu Kα radiation was used to obtain XRD patterns. A Philips Magix-601 X-ray fluorescence (XRF) spectrometer was applied to analyze the chemical composition. A Micromeritics ASAP-2020 analyzer was applied to determine the BET surface areas *via* N_2 adsorption at 77 K. A Micromeritics AutoChem 2920 instrument was used to obtain NH_3-TPD profiles. The pyridine adsorption experiment (Py-IR) was carried out on a Bruker XF808-04 spectrometer. The sample was pressed into a thin self-supporting wafer and pretreated in a vacuum at 673 K for 30 min. Then, the sample adsorbed pyridine for 5 min after cooling to 303 K and the physically adsorbed pyridine was removed in a vacuum at 423 K for 30 min. The mesopore of the catalysts was investigated by using a Tecnai G2F20 (200 kV) high-resolution transmission electron microscope (TEM). The solid-state nuclear magnetic resonance (NMR) experiments were performed on a Bruker Avance III 600 spectrometer equipped with a 14.1 T wide-bore magnet using a 4 mm WVT double resonance MAS probe. ^{27}Al MAS NMR investigations were carried out at 156.4 MHz with a 12 kHz spinning rate. The uptakes of methyl acetate and methyl acrylate on the nano-sized H-ZSM-5 zeolites were measured by an intelligent gravimetric analyzer (IGA). The nano-sized N-H-ZSM-5 catalyst (20 mg, 40–60 mesh) was added to the chamber and evacuated at 573 K for 4 h. The increase in mass with the adsorption of methyl acetate or methyl acrylic over the catalyst was measured at 313 K (5 mbar). Quantification of the effective diffusivity was attained using Fick's second law, to describe the variation of the MA or MAc concentration inside the catalyst as a function of time.

$$\frac{\partial C}{\partial t} = D_{\text{eff}}\left(\frac{\partial^2 C}{\partial x^2}\right) \quad (3)$$

where C is the concentration of MAc or MA inside the particle, t the time, x the distance and D_{eff} the diffusivity. During the initial stage of adsorption, the solution of this equation could be well approximated by:[26,27]

$$\frac{m_t}{m_\infty} = \frac{2}{\sqrt{\pi}}\sqrt{\frac{D_{\text{eff}}}{L^2}}\sqrt{t} \quad (4)$$

where $\frac{m_t}{m_\infty}$ is the normalized MAc or MA uptake, and L is the characteristic diffusion length.

An SU8020 scanning electron microscope (SEM) was utilized to observe the morphology of the catalyst. An SDTQ600 instrument was utilized to perform thermal gravimetric (TGA) analysis. The organic species retained in the spent ZSM-5 catalysts were analyzed by the method of Guisnet.[28] Spent ZSM-5 catalysts were dissolved in a 20 wt% HF solution. After being neutralized with a 5 wt% NaOH solution, the soluble organics were extracted with CH_2Cl_2 which contains 10 ppm C_2Cl_6 as an internal standard, and then analyzed *via* an Agilent 7890B GC-MS instrument which was equipped with an HP-5 capillary column. Diffuse reflectance UV-vis (DR UV-vis) spectra were recorded on a VARIAN Cary-5000 UV-vis-NIR spectrophotometer with $BaSO_4$ used as a reference.

3. Results and discussion

3.1. Catalytic results

The performances of aldol condensation of MAc and HCHO over nano-sized H-type zeolite catalysts (for the characterization results see Fig. 3A, 4A and S1†) with various topologies were compared at 563 K and 0.1 MPa (Fig. 1A). The HCHO conversion and the MA and AA formation rate both follow the order: H-MOR < H-ZSM-35 < H-beta < N-H-ZSM-5. The MFI topology of H-zeolite suggests a better condensation performance. The product distribution over N-H-ZSM-5 in Fig. 1B indicates that except for the hydrolysis and dehydrolysis products (HAc, MeOH, and DME), the others are mostly condensation products MA and AA. In other words, the actual selectivity (without HAc, MeOH, and DME) to MA and AA is up to 95%. The hydrocarbons (HC) are less than 2%, indicating that the MTH reaction over N-H-ZSM-5 is not severe. The performance of two ZSM-5 zeolites with nanocrystals but different Al contents in the aldol condensation reaction was investigated. Fig. 1C shows that N-H-ZSM-5 with a low SiO_2/Al_2O_3 ratio gives a higher condensation activity than N-H-ZSM-5-H with a high SiO_2/Al_2O_3 ratio. It suggests that acid sites should be the catalytic centers for condensation and more acid sites could benefit this reaction. Fig. 1C also depicts that raising the reaction temperature can increase the MA and AA formation rate. As presented in Fig. 1D, the MA and AA formation rate over the nano-sized N-H-ZSM-5 is over 7 times

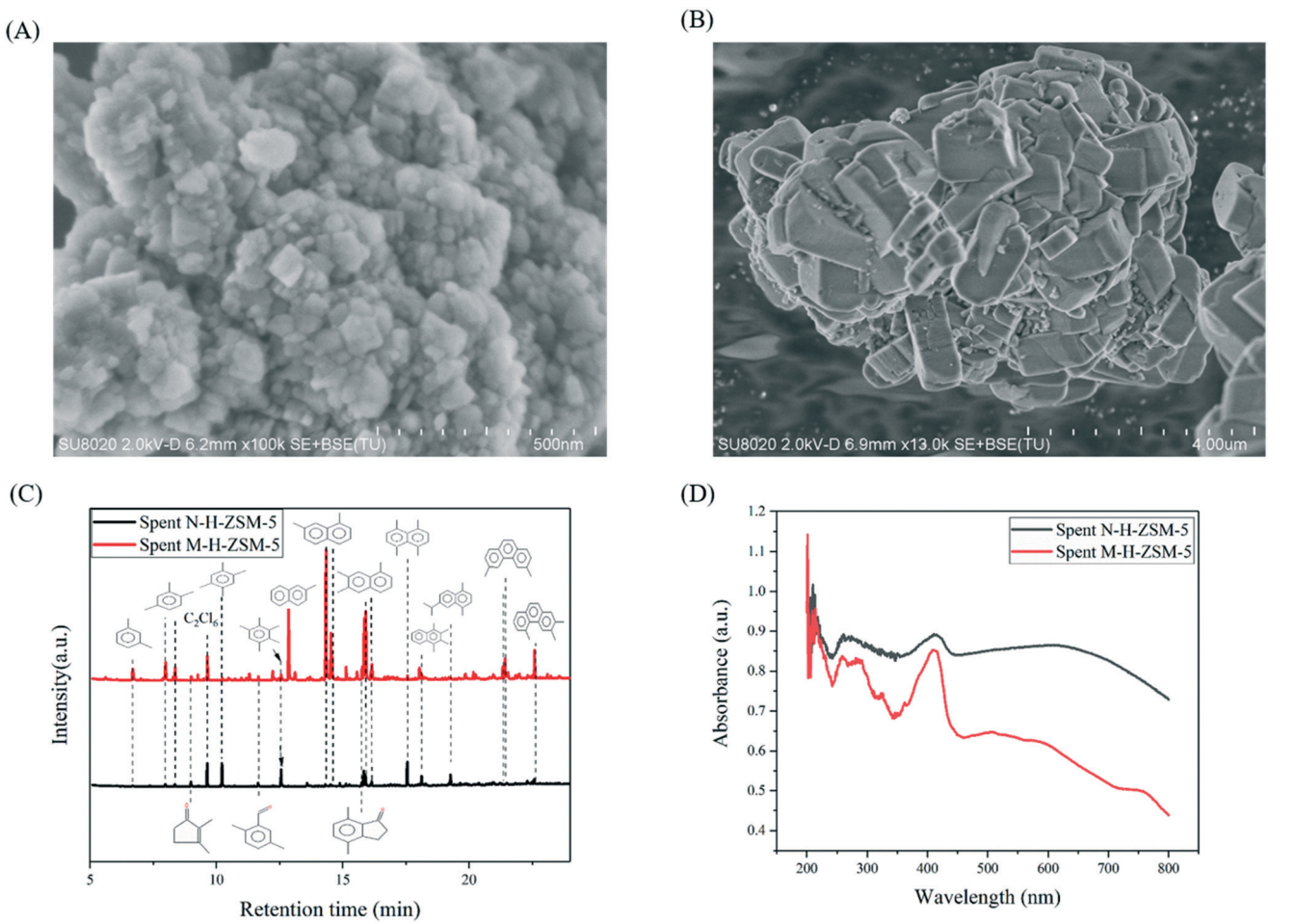

Fig. 3 Results of morphology and coke analysis for ZSM-5 zeolite catalysts. (A) SEM image of N-H-ZSM-5. (B) SEM image of M-H-ZSM-5. (C) Results of GC-MS analysis of the retained organic species in spent catalysts. (D) UV-vis spectra of the spent catalysts.

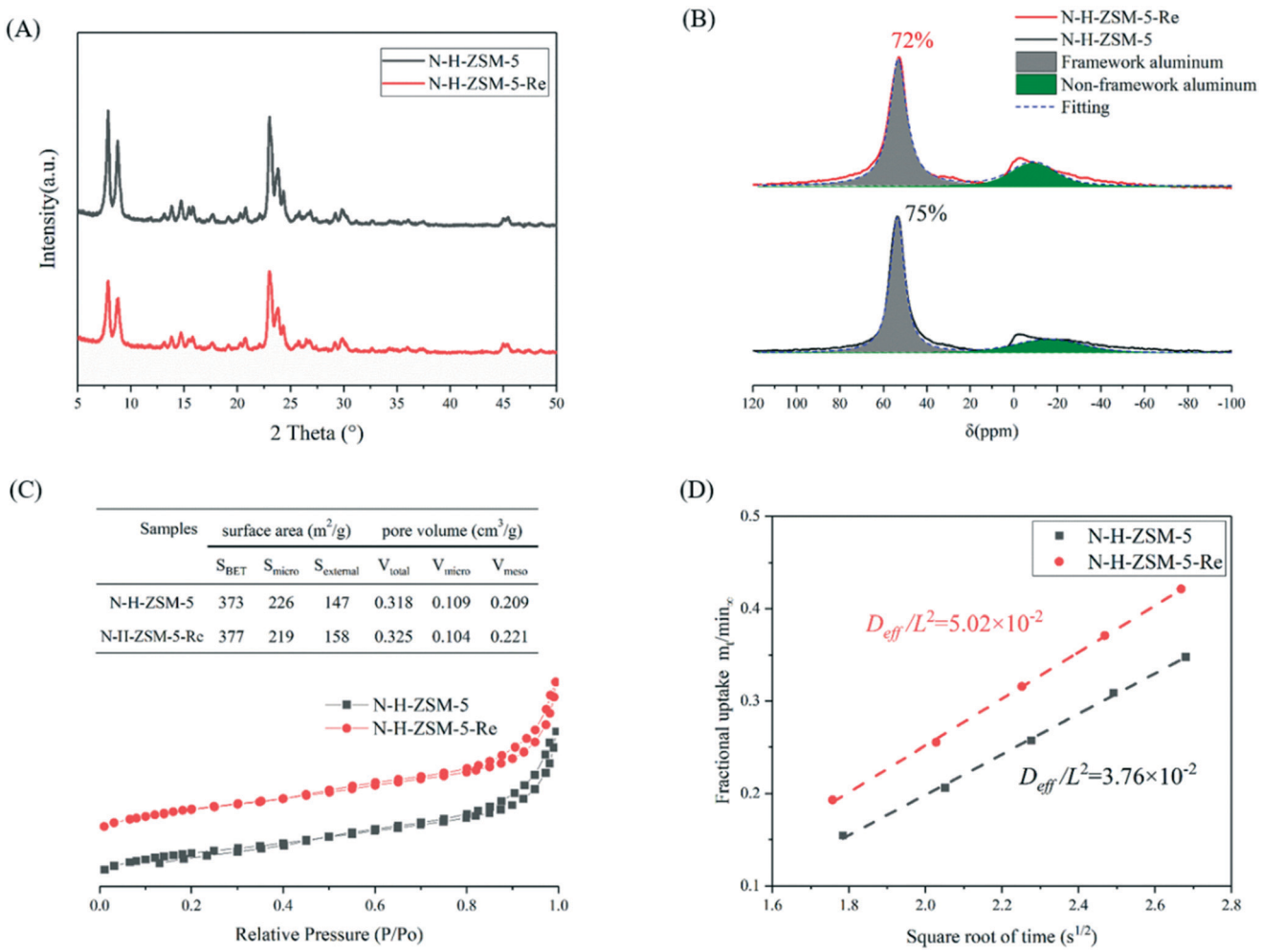

Fig. 4 Results of characterization for N-H-ZSM-5 zeolite catalysts. A: XRD patterns. B: ^{27}Al MAS NMR. C: Py-IR. D: Initial uptake rate of MA in the catalyst measured by IGA (313 K, 5 mbar).

higher than that over the micro-sized M-H-ZSM-5. It can also be observed that the condensation activity for N-H-ZSM-5 decreases quickly during the initial 8 h, then its decreasing rate becomes much lower. However, the condensation activity for M-H-ZSM-5 always keeps a low level. It is noted that N-H-ZSM-5 zeolite with adequate acidity and crystal size shows better catalytic performance than H-ZSM-35 zeolite here, which is different from previous reports[4] due to the lower reaction pressure and using trioxane as the formaldehyde source in this paper. In addition, further investigations on the optimal acidity and crystal size of N-H-ZSM-5 in detail may be necessary to fully evaluate its effect on catalytic behavior in the future study.

Our previous research has proven that when HCHO passes through H-type zeolites, prins, aldol condensations and hydroacylation reactions are prone to simultaneously take place.[22,29] As a result, aromatic hydrocarbons and coke are readily formed, which leads to quick deactivation. Therefore, unmodified H-type zeolites are rarely used directly to study the aldol condensation of MAc and HCHO to synthesize MA and AA. In order to improve the single-pass lifetime of N-H-ZSM-5, we tried to increase the reaction temperature programmatically to compensate for the decrease in the aldol condensation activity. Interestingly, the single-pass lifetime of fresh N-H-ZSM-5, during which the MA and AA formation rate is more than 0.9 mmol g^{-1} h^{-1}, can reach up to 53 h (Fig. 2A). The deactivated N-H-ZSM-5 was regenerated by calcination in air at 823 K. Unexpectedly, the aldol condensation activity is slightly improved after the first regeneration. As shown in Fig. 2A and B, both the aldol condensation activity and the single-pass lifetime can be continuously increased after the second and third regenerations. Therefore, we speculate that the actual total lifetime of the N-H-ZSM-5 catalyst could be much longer than 226 hours in Fig. 2A, which is of great significance for industrial applications.

3.2. Structural characterization

As shown in Fig. 3A and B, N-H-ZSM-5 is made up of about 50 nm particles, while M-H-ZSM-5 is composed of 2–5 μm hexagonal crystals. Combined with TGA results in Fig. S3† and catalytic results in Fig. 1D, it can be observed that

although the amount of coke in the spent N-H-ZSM-5 is approximately twice higher than that in the spent M-H-ZSM-5, the MA and AA formation rate for the former is 7 times higher than that for the latter one. This indicates that the nano-sized N-H-ZSM-5 is more resistant to coke. The two spent ZSM-5 zeolite catalysts were dissolved with HF, then the soluble retained organic species were extracted with CH_2Cl_2, and analyzed by GC-MS. As presented in Fig. 3C, compared with the spent N-H-ZSM-5, the spent M-H-ZSM-5 contains more polyaromatic hydrocarbons such as naphthalene and phenanthrene. These soluble polyaromatic hydrocarbons are too large to block the mouth of micropores,[30] and finally cause deactivation. UV-vis spectroscopy was employed to identify the insoluble and highly condensed polyaromatic hydrocarbons (Fig. 3D). The broad band at 620 nm is related to the formation of polyaromatic hydrocarbons such as pyrene,[31,32] which are usually located on the external surface of zeolite. It is obvious that the amount of insoluble polyaromatic hydrocarbons in the spent N-H-ZSM-5 is higher than that in the spent M-H-ZSM-5, which indicates that the former catalyst possesses a large capacity to accommodate big-sized polyaromatic coke.

The XRD patterns (Fig. 4A) demonstrate that the crystallinity of N-H-ZSM-5 is almost unchanged after 4 regeneration runs. The results of NH_3-TPD (Fig. S4†) and Py-FTIR (Fig. S5†) show that the amount and the type of acid sites of N-H-ZSM-5 can be largely maintained after regeneration. The ^{27}Al MAS NMR results (Fig. 4B) verify that the ratio of framework Al in the regenerated N-H-ZSM-5 is only slightly decreased. These characterization results above prove that the crystal structure and catalytic center (acid sites) are both stable in the reaction and regeneration atmosphere. This may overcome the inherent shortcomings of conventional base or base–acid bifunctional catalysts. The catalytic centers of these catalysts are prone to be lost in an acidic and water atmosphere.[8,17] In order to investigate the essential causes of the improvement of condensation activity after regeneration in Fig. 2A and B, the N_2 physical adsorption and desorption results are compared (Fig. 4C). The external area and mesopore volume of N-H-ZSM-5 are both increased after reaction and regeneration. The TEM results (Fig. S6†) also show that apparent intracrystalline mesopores occurred in the regenerated N-H-ZSM-5. We speculate that the activity increment may come from the improvement of diffusion performance. The diffusion performances of product MA and reactant MAc were evaluated by the IGA method (Fig. 4D and S7†). The value of the diffusion time constant (D_{eff}/L^2) is a good indicator of the mass transfer properties.[26,27] It is quite clear that the calculated D_{eff}/L^2 for MA is enhanced, indicating that diffusion properties are indeed improved after reaction and regeneration. This IGA result further confirms our inference.

4. Conclusion

In summary, the efficient and long-term stable conversion of MAc and HCHO to MA and AA can be simultaneously achieved over the nano-sized N-H-ZSM-5 zeolite catalyst. The total lifetime of N-H-ZSM-5 reaches up to 226 h by three regeneration runs with the MA and AA formation rate being more than 0.9 mmol g^{-1} h^{-1}. The aldol condensation activity and the single-pass lifetime can even be continuously increased after each regeneration. For N-H-ZSM-5, the large capacity to hold big-sized polyaromatic coke, the good structural stability during the reaction and regeneration, and the gradually improved diffusion performance after regeneration lead to such excellent aldol condensation performances. This aldol condensation result is promising for industrial applications.

Author contributions

Conceptualization: W. L. Z., Y. M. N., and M. G. X.; investigation: M. G. X., Y. M. N., X. D. F., H. C. L., Z. Y. C., X. N. D., and L. Y. W.; validation: M. G. X. and Y. M. N.; writing – original draft: M. G. X.; visualization: M. G. X. and X. D. F.; writing – review & editing: W. L. Z., Y. M. N., H. C. L., and Z. Y. C.; supervision: W. L. Z., Y. M. N., and H. C. L.

Conflicts of interest

There are no conflicts to declare.

Acknowledgements

We acknowledge the financial support from the National Natural Science Foundation of China (Grant No. 21978285, 21972141, 21991094 and 21991090), the "Transformational Technologies for Clean Energy and Demonstration", Strategic Priority Research Program of the Chinese Academy of Sciences (Grant No. XDA21030100), the Dalian High Level Talent Innovation Support Program (2017RD07), and the National Special Support Program for High Level Talents (SQ2019RA2TST0016). We acknowledge Mrs. Yanli He and Mr. Yijun Zheng for their help in the characterization of the catalysts.

Notes and references

1 M. M. Bettahar, G. Costentin, L. Savary and J. C. Lavalley, *Appl. Catal., A*, 1996, **145**, 1–48.
2 W. Fang, Q. J. Ge, J. F. Yu and H. Y. Xu, *Ind. Eng. Chem. Res.*, 2011, **50**, 1962–1967.
3 B. Y. Jo, S. S. Kum and S. H. Moon, *Appl. Catal., A*, 2010, **378**, 76–82.
4 Z. L. Ma, X. G. Ma, H. C. Liu, Y. L. He, W. L. Zhu, X. W. Guo and Z. M. Liu, *Chem. Commun.*, 2017, **53**, 9071–9074.
5 Y. Traa, *Chem. Commun.*, 2010, **46**, 2175–2187.
6 A. I. Biaglow, J. Sepa, R. J. Gorte and D. White, *J. Catal.*, 1995, **151**, 373–384.
7 T. Yan, S. Yao, W. Dai, G. Wu, N. Guan and L. Li, *Chin. J. Catal.*, 2021, **42**, 595–605.
8 J. B. Yan, C. L. Zhang, C. L. Ning, Y. Tang, Y. Zhang, L. L. Chen, S. Gao, Z. L. Wang and W. X. Zhang, *J. Ind. Eng. Chem.*, 2015, **25**, 344–351.

9 T. He, Y. X. Qu and J. D. Wang, *Catal. Lett.*, 2019, **149**, 373–389.
10 T. He, Y. X. Qu and J. D. Wang, *Ind. Eng. Chem. Res.*, 2018, **57**, 2773–2786.
11 G. L. Zhang, H. H. Zhang, D. Yang, C. S. Li, Z. J. Peng and S. J. Zhang, *Catal. Sci. Technol.*, 2016, **6**, 6417–6430.
12 Q. Bao, T. T. Bu, J. B. Yan, C. L. Zhang, C. L. Ning, Y. Zhang, M. M. Hao, W. X. Zhang and Z. L. Wang, *Catal. Lett.*, 2017, **147**, 1540–1550.
13 M. Ai, *J. Catal.*, 1987, **107**, 201–208.
14 X. Z. Feng, B. Sun, Y. Yao, Q. Su, W. J. Ji and C. T. Au, *J. Catal.*, 2014, **314**, 132–141.
15 X. P. Guo, D. Yang, C. C. Zuo, Z. J. Peng, C. S. Li and S. J. Zhang, *Ind. Eng. Chem. Res.*, 2017, **56**, 5860–5871.
16 D. Yang, C. Sararuk, H. Wang, S. J. Zhang, Z. X. Li and C. S. Li, *Ind. Eng. Chem. Res.*, 2018, **57**, 93–100.
17 D. Yang, G. Wang, H. Wu, X. P. Guo, S. J. Zhang, Z. X. Li and C. S. Li, *Catal. Today*, 2018, **316**, 122–128.
18 R. Simancas, A. Chokkalingam, S. P. Elangovan, Z. Liu, T. Sano, K. Iyoki, T. Wakihara and T. Okubo, *Chem. Sci.*, 2021, **12**, 7677–7695.
19 C. C. Zuo, T. T. Ge, X. P. Guo, C. S. Li and S. J. Zhang, *Microporous Mesoporous Mater.*, 2018, **256**, 58–66.
20 Z. L. Ma, X. G. Ma, H. C. Liu, W. L. Zhu, X. W. Guo and Z. M. Liu, *Chin. J. Catal.*, 2018, **39**, 1129–1137.
21 Z. Ma, X. Ma, Y. Ni, H. Liu, W. Zhu, X. Guo and Z. Liu, *Chin. J. Catal.*, 2018, **39**, 1762–1769.
22 Y. Ni, W. Zhu and Z. Liu, *ACS Catal.*, 2019, **9**, 11398–11403.
23 Y. Ni, K. Wang, W. Zhu and Z. Liu, *Chem Catalysis*, 2021, **1**, 383–392.
24 Z. Y. Chen, Y. M. Ni, Y. C. Zhi, F. L. Wen, Z. Q. Zhou, Y. X. Wei, W. L. Zhu and Z. M. Liu, *Angew. Chem., Int. Ed.*, 2018, **57**, 12549–12553.
25 Z. Zhou, H. Liu, Y. Ni, F. Wen, Z. Chen, W. Zhu and Z. Liu, *J. Catal.*, 2021, **396**, 360–373.
26 K. Cao, D. Fan, S. Zeng, B. Fan, N. Chen, M. Gao, D. Zhu, L. Wang, P. Tian and Z. Liu, *Chin. J. Catal.*, 2021, **42**, 1468–1477.
27 D. Jin, G. Ye, J. Zheng, W. Yang, K. Zhu, M.-O. Coppens and X. Zhou, *ACS Catal.*, 2017, **7**, 5887–5902.
28 M. Guisnet and P. Magnoux, *Appl. Catal.*, 1989, **54**, 1–27.
29 Y. Ni, W. Zhu and Z. Liu, *J. Energy Chem.*, 2021, **54**, 174–178.
30 F. Bleken, W. Skistad, K. Barbera, M. Kustova, S. Bordiga, P. Beato, K. P. Lillerud, S. Svelle and U. Olsbye, *Phys. Chem. Chem. Phys.*, 2011, **13**, 2539–2549.
31 V. Van Speybroeck, K. Hemelsoet, K. De Wispelaere, Q. Qian, J. Van der Mynsbrugge, B. De Sterck, B. M. Weckhuysen and M. Waroquier, *ChemCatChem*, 2013, **5**, 173–184.
32 E. Borodina, F. Meirer, I. Lezcano-Gonzalez, M. Mokhtar, A. M. Asiri, S. A. Al-Thabaiti, S. N. Basahel, J. Ruiz-Martinez and B. M. Weckhuysen, *ACS Catal.*, 2015, **5**, 992–1003.